J|A|C|S ARTICLES

Published on Web 07/21/2010

Largest Molecular Clusters in the Supertetrahedral T*n* Series

Tao Wu,[†] Le Wang,[†] Xianhui Bu,[‡] Victoria Chau,[†] and Pingyun Feng*,[†]

Department of Chemistry, University of California, Riverside, California 92521, and Department of Chemistry and Biochemistry, California State University, 1250 Bellflower Boulevard, Long Beach, California 90840

Received March 30, 2010; E-mail: pingyun.feng@ucr.edu

Abstract: Supertetrahedral T*n* clusters are exact fragments of cubic ZnS-type lattice and are often formed *in situ* as building units for the construction of 3-D open-framework chalcogenide materials. Small T*n* clusters can also be synthesized in discrete forms, allowing them to exist as soluble species in solution. In addition to their tunable electronic and optical properties, these soluble clusters can be used as precursors for the synthesis of porous semiconducting and optical materials. However, the synthesis of large T*n* clusters is a significant challenge, and for several decades prior to this work, the size of the discrete T*n* cluster remained at T3, with only 10 metal sites (e.g., $[Cd_{10}S_4(SPh)_{16}]^{4-}$ and $[M_5Sn_5S_{20}]^{10-}$, M = Zn, Co). Here we report a family of discrete chalcogenide T4 clusters ($[M_xGa_{18-x}Sn_2Q_{35}]^{12-}$, $x = 2$ or 4; M = Mn, Cu, Zn; Q = S, Se) whose discovery resulted from an unusual phase transformation from a 3-D T4 covalent framework into 0-D T4 molecular clusters. The driving force for such a transformation is the perfect match in both charge density and geometry between chalcogenide clusters and protonated amine, leading to the higher stability of isolated clusters. The perfect match is achieved by using complex quaternary compositions to maximize charge tunability of the cluster. These T4 clusters are the largest molecular T*n* clusters known to date and can be made in various compositions showing tunable band structures in both solution and solid state.

1. Introduction

Since the first synthesis of chalcogenide open-framework materials in 1989,[1] research on crystalline porous chalcogenide frameworks has attracted great attention[2−4] because such materials are capable of integrating porosity with semiconductivity and have many potential applications. Unlike crystalline porous materials based on inorganic oxide frameworks[5] (e.g., zeolites) or more recently developed porous coordination polymers (also called metal−organic frameworks, MOFs),[6−8] chalcogenide open frameworks have distinct structural features, and many of them are composed of nanosized tetrahedral clusters.[3] Such clusters can behave as artificial tetrahedral atoms to allow the creation of semiconducting zeolite-like four-connected porous frameworks.[9] On the other hand, these clusters can also be considered as the smallest possible semiconductor quantum dots, and because of their precisely defined composition and structure, they may exhibit unique properties in addition to serving as model systems for less-well-defined colloidal nanoparticles.[10,11] Such a close relevance of chalcogenide clusters to crystalline porous semiconductors and semiconductor

[†] University of California, Riverside.
[‡] California State University.

(1) Bedard, R. L.; Wilson, S. T.; Vail, L. D.; Bennett, J. M.; Flanigen, E. M. *Stud. Surf. Sci. Catal. A* **1989**, *49*, 375–387.
(2) (a) Ding, N.; Kanatzidis, M. G. *Nature Chem.* **2010**, *2*, 187–191. (b) Mertz, J.; Ding, N.; Kanatzidis, M. G. *Inorg. Chem.* **2009**, *48*, 10898–10900. (c) Ding, N.; Kanatzidis, M. G. *Angew. Chem., Int. Ed.* **2006**, *45*, 1397–1401. (d) Ding, N.; Chung, D.-Y.; Kanatzidis, M. G. *Chem. Commun.* **2004**, 1170–1171. (e) Feng, P.; Bu, X.; Zheng, N. *Acc. Chem. Res.* **2005**, *38*, 293–303. (f) Bu, X.; Zheng, N.; Feng, P. *Chem.—Eur. J.* **2004**, *10*, 3356–3362.
(3) Li, H.; Laine, A.; O'Keeffe, M.; Yaghi, O. M. *Science* **1999**, *283*, 1145–1147.
(4) (a) Dehnen, S.; Melullis, M. *Coord. Chem. Rev.* **2007**, *251*, 1259–1280. (b) Vaqueiro, P. *Inorg. Chem.* **2008**, *47*, 20–22. (c) Vaqueiro, P.; Romero, M. L. *J. Phys. Chem. Solids* **2006**, *68*, 1239–1243. (d) Dehnen, S.; Brandmayer, M. K. *J. Am. Chem. Soc.* **2003**, *125*, 6618–6619. (e) Palchik, O.; Lyer, R. G.; Liao, J. H.; Kanatzidis, M. G. *Inorg. Chem.* **2003**, *42*, 5052–5054. (f) Zimmermann, C.; Melullis, M.; Dehnen, S. *Angew. Chem., Int. Ed.* **2002**, *41*, 4269–4272. (g) Zimmermann, C.; Anson, C. E.; Weigend, F.; Clérac, R.; Dehnen, S. *Inorg. Chem.* **2005**, *44*, 5686–5695. (h) Vaqueiro, P.; Romero, M. L. *Chem. Commun.* **2007**, 3282–3284. (i) Vaqueiro, P.; Romero, M. L. *Inorg. Chem.* **2009**, *48*, 810–812.
(5) (a) Cheetham, A. K.; Férey, G.; Loiseau, T. *Angew. Chem., Int. Ed.* **1999**, *38*, 3268–3292. (b) Davis, M. *E Nature* **2002**, *417*, 813–821.
(6) (a) Ma, L.; Abney, C.; Lin, W. *Chem. Soc. Rev.* **2009**, *38*, 1248–1256. (b) Xie, Z.; Ma, L.; deKrafft, K. E.; Jin, A.; Lin, W. *J. Am. Chem. Soc.* **2010**, *132*, 922–923. (c) deKrafft, K. E.; Xie, Z.; Cao, G.; Tran, S.; Ma, L.; Zhou, O. Z.; Lin, W. *Angew. Chem., Int. Ed.* **2009**, *48*, 9901–9904.
(7) (a) Férey, G. *Chem. Soc. Rev.* **2008**, *37*, 191–214. (b) Férey, G.; Serre, C. *Chem. Soc. Rev.* **2009**, *38*, 1380–1399. (c) Férey, G.; Draznieks, C. M.; Serre, C.; Millange, F. *Acc. Chem. Res.* **2005**, *38*, 217–225.
(8) (a) O'Keeffe, M. *Chem. Soc. Rev.* **2009**, *38*, 1215–1217. (b) Li, J.-R.; Kuppler, R. J.; Zhou, H.-C. *Chem. Soc. Rev.* **2009**, *38*, 1477–1504. (c) Farha, O. K.; Malliaks, C. D.; Kanatzidis, M. G.; Hupp, J. T. *J. Am. Chem. Soc.* **2010**, *132*, 950–952. (d) Kitagawa, S.; Kitaura, R.; Noro, S. *Angew. Chem., Int. Ed.* **2004**, *43*, 2334–2375. (e) Murray, L. J.; Dincă, M.; Long, J. R. *Chem. Soc. Rev.* **2009**, *38*, 1294–1314. (f) Uemura, T.; Yanai, N.; Kitagawa, S. *Chem. Soc. Rev.* **2009**, *38*, 1228–1236.
(9) Zheng, N.; Bu, X.; Wang, B.; Feng, P. *Science* **2002**, *298*, 2366–2369.
(10) (a) Herron, N.; Calabrese, J. C.; Farneth, W. E.; Wang, Y. *Science* **1993**, *259*, 1426–1428. (b) Zheng, N.; Bu, X.; Lu, H.; Zhang, Q.; Feng, P. *J. Am. Chem. Soc.* **2005**, *127*, 11963–11965.
(11) Corrigan, J. F.; Fuhr, O.; Fenske, D. *Adv. Mater.* **2009**, *21*, 1867–1871.

quantum dots places them in a unique family of materials whose study will have significant multidisciplinary impacts.

There are now four well-known series of tetrahedral chalcogenide nanoclusters: supertetrahedral cluster (T*n*), pentasupertetrahedral cluster (P*n*), capped supertetrahedral (C*n*) cluster, and super-supertetrahedral cluster (T*p*,*q*) (*n*, *p*, and *q* are related to the size of the cluster and in known clusters range 1−5 for T*n*, 1−2 for P*n*, and 1−3 for C*n* clusters).[3,12] Examples of T2, P1, C1, and C2 clusters are $[Cd_4(SPh)_{10}]^{2-}$ (or $[M_4Q_{10}]^{4-}$, M = Ge, Sn; Q = Se, S), $[Cd_8S(SPh)_{16}]^{2-}$ (or $[M_4Sn_4Q_{17}]^{10-}$ (M = Zn, Mn, Co, Fe; Q = Se, S),[4d−f] $[Cd_{17}S_4(SPh)_{28}]^{2-}$, and $[Cd_{32}S_{14}(SPh)_{36}(DMF)_4]$, respectively. Among these clusters, supertetrahedral T*n* clusters are the most fundamental series, and other series of clusters can be geometrically derived from T*n* clusters.

For many years, the synthesis of large, crystallographically defined chalcogenide clusters (i.e., to increase *n*) has remained a formidable challenge. For supertetrahedral T*n* clusters, it has actually been more difficult to create discrete molecular clusters than to synthesize covalently linked clusters. For example, T3 clusters (e.g., $[Cd_{10}S_4(SPh)_{16}]^{4-}$)[13] have remained the largest discrete supertetrahedral T*n* clusters for many years, even though some new compositions have recently been made (e.g., $[M_5Sn_5S_{20}]^{10-}$, M = Zn, Co),[4g] and both T4 and T5 clusters are known in extended frameworks.[2e]

There has always been a strong interest in discrete molecular clusters that can serve as precursors to allow the more rational construction of porous frameworks through modular assembly processes, in a way similar to the construction of coordination polymers.[14−17] Discrete clusters are also more directly comparable to semiconductor nanoparticles in terms of properties such as quantum confinement effects. Furthermore, discrete soluble clusters are amenable for solution processing into various forms such as thin films, functionalized semiconducting mesoporous structure,[18] or porous gels and aerogels.[19,20]

One of the key structural features of tetrahedral chalcogenide clusters, which is also related to the difficulty in synthesizing them, is their usually negative charge that increases dramatically as the size of the cluster gets bigger. The reason for the negative charge is that, while the coordination sphere of tetrahedral metal sites is saturated with four S^{2-}/Se^{2-} sites, surface S^{2-}/Se^{2-} sites are bonded to fewer than four metal sites, leading to excess anionic sites (i.e., anion/metal > 1). As the cluster gets larger, the increase in the surface area of the cluster leads to a large number of such underbonded S^{2-}/Se^{2-} sites, which contribute to a dramatic increase in the magnitude of the negative charge per cluster. Thus, a key strategy in synthesizing large clusters is to find methods to stabilize or lower the large negative charge.

There are two common ways to reduce the negative charge: incorporating surface organic ligands or introducing surface high-valent (3+ or 4+) metal cations. For chalcogenide clusters made of entirely divalent metal ions such as Cd^{2+}, the charge reduction is achieved through covalently attached surface organic ligands (in the form of thiolates or selenolates). For example, the T3 $[Cd_{10}S_{20}]^{20-}$ cluster only exists with its edge and corner S^{2-} sites bonded to organic groups (e.g., T3 $[Cd_{10}S_4(SPh)_{16}]^{4-}$).[13] The T4 cluster in this type of composition is not known yet.

When high-valent metal ions (e.g., Ga^{3+} or In^{3+}) are present on the surface of clusters, the valence requirements of surface S^{2-}/Se^{2-} can be satisfied even if the S^{2-}/Se^{2-} site is bonded to fewer than four metal sites.[21−24] This eliminates or reduces the need for organic ligands, which helps to form inorganic supertetrahedral chalcogenide clusters such as $In_{10}S_{18}^{6-}$. Furthermore, there have been reports of some very interesting clusters that contain both trivalent cations and organic ligands (generally at the corners of the cluster, e.g., T3 cluster $[Ga_{10}S_{16}(C_7H_9N)_4]^{2-}$, C_7H_9N = 3,5-lutidine)[4h,i] Such clusters make use of both types of charge reduction mechanisms.

Tetravalent metals such as Sn^{4+} have had an interesting history in terms of their roles in cluster and framework formation. In the early years of open-framework chalcogenides, such tetravalent metal ions were selected as the primary framework metal species in efforts to emulate silica-like structures.[1] Low-valent metal ions (e.g., Mn^{2+}) were initially used to play the secondary role, such as cross-linking small clusters (e.g., $Ge_4S_{10}^{4-}$) into extended frameworks, instead of forming heterometallic clusters with Ge−S.[14] Later, it was found that Sn^{4+} could participate in the formation of inorganic clusters such as P1 and T3, in combination with divalent metal ions, as demonstrated by the groups of Dehnen and Kanatzidis.[4d−g] These clusters that usually have a molar ratio of 1 between Sn^{4+} and M^{2+} (e.g., Zn^{2+}) are early examples that demonstrate the charge reduction role of tetravalent metal ions in the formation of tetrahedral clusters.[4d−g] Our own work in $M^{4+}/M^{3+}/X^{2-}$ systems (M^{4+} = Ge^{4+}, Sn^{4+}; M^{3+} = Ga^{3+}, In^{3+}; X^{2-} = S^{2-}, Se^{2-}) highlighted the charge reduction role of M^{4+} in the formation of T2 clusters.[9] Furthermore, a very recent example ($[Sn_4Ga_4Zn_2Se_{20}]^{8-}$) also contains Sn^{4+} at the corner of a discrete T3 cluster, even though it needs to be stabilized by a covalently attached metal complex ($[(TEPA)Mn]^{2+}$, TEPA = tetraethylenepentamine).[25]

The aforementioned examples demonstrate the feasibility to synthesize large supertetrahedral clusters through the incorporation of high-valent metal ions such as In^{3+} and Sn^{4+}. However, the relative concentrations of M^{4+}, M^{3+}, and M^{2+} (or M^{+}) need

(12) Li, H.; Kim, J.; O'Keeffe, M.; Yaghi, O. M. *Angew. Chem., Int. Ed.* **2003**, *42*, 1819–1821.
(13) (a) Choy, A.; Craig, D.; Dance, I.; Scudder, M. L. *J. Chem. Soc., Chem. Commun.* **1982**, 1246–1247. (b) Dance, I. G.; Chony, A.; Scudder, M. L. *J. Am. Chem. Soc.* **1984**, *106*, 6285–6295.
(14) Yaghi, O. M.; Sun, Z.; Richardson, D. A.; Groy, T. L. *J. Am. Chem. Soc.* **1994**, *116*, 807–808.
(15) Vaqueiro, P.; Romero, M. L. *J. Am. Chem. Soc.* **2008**, *130*, 9630–9631.
(16) (a) Tan, K.; Darovsky, A.; Parise, J. B. *J. Am. Chem. Soc.* **1995**, *117*, 7039–7040. (b) Cahill, C. L.; Parise, J. B. *Chem. Mater.* **1997**, *9*, 807–811.
(17) Ahari, H.; Garcia, A.; Kirkby, S.; Ozin, G. A.; Young, D.; Lough, A. J. *J. Chem. Soc., Dalton Trans.* **1998**, 2023–2027.
(18) (a) Wachhold, M.; Rangan, K. K.; Billinge, S. J. L.; Petkov, V.; Heising, J.; Kanatzidis, M. G. *Adv. Mater.* **2000**, *12*, 85–91. (b) Ding, N.; Takabayashi, Y.; Solari, P. L.; Prassides, K.; Pcionek, R. J.; Kanatzidis, M. G. *Chem. Mater.* **2006**, *18*, 4690–4699.
(19) Mohanan, J. L.; Arachchige, I. U.; Brock, S. L. *Science* **2005**, *307*, 397–400.
(20) (a) Bag, S.; Trikalitis, P. N.; Chupas, P. J.; Armatas, G. S.; Kanatzidis, M. G. *Science* **2007**, *317*, 490–493. (b) Bag, S.; Arachchige, I. U.; Kanatzidis, M. G. *J. Mater. Chem.* **2008**, *18*, 3628–3632.
(21) Li, H.; Kim, J.; Groy, T. L.; O'Keeffe, M.; Yaghi, O. M. *J. Am. Chem. Soc.* **2001**, *123*, 4867–4868.
(22) Wang, C.; Li, Y.; Bu, X.; Zheng, N.; Zivkovic, O.; Yang, C.-S.; Feng, P. *J. Am. Chem. Soc.* **2001**, *123*, 11506–11507.
(23) (a) Wang, C.; Li, Y.; Bu, X.; Zheng, N.; Zivkovic, O.; Yang, C.-S.; Feng, P. *J. Am. Chem. Soc.* **2001**, *123*, 11506–11507. (b) Bu, X.; Zheng, N.; Li, Y.; Feng, P. *J. Am. Chem. Soc.* **2002**, *124*, 12646–12647. (c) Wang, L.; Wu, T.; Zuo, F.; Zhao, X.; Bu, X.; Wu, J.; Feng, P. *J. Am. Chem. Soc.* **2010**, *132*, 3283–3285.
(24) Su, W.; Huang, X.; Li, J.; Fu, H. *J. Am. Chem. Soc.* **2002**, *124*, 12944–12945.
(25) Xu, G.-H.; Guo, P.; Song, S.-Y.; Zhang, H.-J.; Wang, C. *Inorg. Chem.* **2009**, *48*, 4628–4630.

Table 1. Summary of Crystal Data and Refinement Parameters for OCF-5s and OCF-40s[a]

name[b]	formula	symmetry group	*a* (Å)	*c* (Å)	*R* (F)
OCF-5-CuGaSnSe-DPM	$[Cu_2Ga_{16}Sn_2Se_{33}]\cdot$(template)[c]	$I4_1/acd$	23.9286(2)	42.0821(5)	5.85
OCF-5-ZnGaSnSe-2-MPR	$[Zn_4Ga_{14}Sn_2Se_{33}]\cdot$(template)	$I4_1/acd$	24.1584(12)	41.931(4)	4.88
OCF-5-ZnGaSnSe-3-MPR	$[Zn_4Ga_{14}Sn_2Se_{33}]\cdot$(template)	$I4_1/acd$	24.0693(3)	42.2601(10)	7.33
OCF-40-CuGaSnSe-PR	$[Cu_2Ga_{16}Sn_2Se_{35}]\cdot 12(C_5NH_{12})$[d]	$I\bar{4}3m$	18.8019(1)	18.8019(1)	3.28
OCF-40-ZnGaSnSe-PR	$[Zn_4Ga_{14}Sn_2Se_{35}]\cdot 12(C_5NH_{12})$	$I\bar{4}3m$	18.8951(1)	18.8951(1)	4.08
OCF-40-MnGaSnSe-PR	$[Mn_4Ga_{14}Sn_2Se_{35}]\cdot 12(C_5NH_{12})$	$I\bar{4}3m$	18.8626(2)	18.8626(2)	4.17
OCF-40-CuGaSnSe-4-MPR	$[Cu_2Ga_{16}Sn_2Se_{35}]\cdot 12(C_6NH_{14})$[e]	$I\bar{4}3m$	19.387(2)	19.387(2)	
OCF-40-ZnGaSnSe-4-MPR	$[Zn_4Ga_{14}Sn_2Se_{35}]\cdot 12(C_6NH_{14})$	$I\bar{4}3m$	19.2020(3)	19.2020(3)	
OCF-40-CuGaSnS-PR	$[Cu_2Ga_{16}Sn_2S_{35}]\cdot 12(C_5NH_{12})$	$I\bar{4}3m$	18.4280(3)	18.4280(3)	5.38
OCF-40-ZnGaSnS-PR	$[Zn_4Ga_{14}Sn_2S_{35}]\cdot 12(C_5NH_{12})$	$I\bar{4}3m$	18.2580(15)	18.2580(15)	5.84
OCF-40-MnGaSnS-PR	$[Mn_4Ga_{14}Sn_2S_{35}]\cdot 12(C_5NH_{12})$	$I\bar{4}3m$	18.3783(11)	18.3783(11)	4.26

[a] Structures were solved from single-crystal data collected at 150 K on a SMART CCD diffractometer with Mo Kα. $R(F) = \sum||F_o| - |F_c||/\sum|F_o|$, with $F_o > 4.0\sigma(F)$. [b] PR = piperidine, $C_5H_{11}N$; 2-MPR = 2-methylpiperidine, $C_6H_{13}N$; 3-MPR = 3-methylpiperidine, $C_6H_{13}N$; 4-MPR = 4-methylpiperidine, $C_6H_{13}N$; DPM = dipiperidinomethane, $C_{11}H_{22}N_2$. [c] For OCF-5, framework atoms are located, and guest protonated amine molecules (template) are disordered. [d] C_5NH_{12} is the formula of piperidinium. [e] C_6NH_{14} is the formula of 4-methylpiperidinium.

to be carefully controlled, because M^{4+} and M^{3+} could suppress the formation of tetrahedrally coordinated S^{2-} (or Se^{2-}) sites (e.g., M_4S) that are essential for the formation of large clusters. On the other hand, control of the cluster charge is only one aspect in the cluster synthesis. Even more difficult is the crystallization of clusters, because it requires proper charge-balancing species that also need to possess suitable geometries to fill the intercluster cavities. Given the great difficulty in finding such charge-balancing species from a large library of organic molecules, one of the best ways to induce the crystallization of large clusters is to use a complex chemical system that contains multiple charge-complementary metal ions in different oxidation states (e.g., $M^+/M^{3+}/M^{4+}$ or $M^{2+}/M^{3+}/M^{4+}$; M^+ or M^{2+} is essential for the formation of the core of the cluster, while M^{3+}/M^{4+} serves to meet the valence requirement of underbonded surface anions). By allowing the possibility to adjust the ratio of these different metal ions within the cluster, it would create a degree of freedom for the cluster to self-adjust its charge density to match that of the organic cationic species during crystallization. This strategy, which further extends the earlier methods in M^{4+}/M^{2+},[4d–g] M^{4+}/M^{3+},[9] $M^{4+}/M^{3+}/M^{2+}$,[25] and related systems, is similar to that used for the synthesis of zeolite-like cobalt aluminophosphates, in which the ratio between Co^{2+} and Al^{3+} within the phosphate framework can be adjusted to tune the framework negative charge so that the inorganic framework has a better chance of matching the charge density of organic structure-directing agents for crystallization.[26] The synthesis of $[Sn_4Ga_4Zn_2Se_{20}]^{8-}$ by Wang et al. represents one successful example.[25] It is worth noting that the use of such trimetal systems can also lead to other possibilities, as shown by the synthesis of OCF-42, in which the framework was constructed by connecting T2 ($Ga^{3+}/Sn^{4+}/Se^{2-}$) clusters with T4 ($Zn^{2+}/Ga^{3+}/Se^{2-}$).[27]

Here we report the application of the above synthetic strategy in synthesizing a family of discrete supertetrahedral T4 clusters. A total of eight distinct crystalline phases containing discrete T4 clusters, but differing in chemical compositions, have been synthesized, all of which are denoted as OCF-40s (OCF stands for organically directed chalcogenide frameworks). These clusters can be made as both sulfides and selenides (Table 1). Different combinations of metal cations have also been achieved (Table 1), further increasing the level of control over their electronic band structures. OCF-40s represent the largest isolated supertetrahedral (T*n* series) chalcogenide nanoclusters known to date. To better appreciate the extraordinary synthetic conditions under which these record-breaking clusters are synthesized, we also report here three related framework structures (collectively denoted as OCF-5s here) in which T4 clusters (with previously unknown chemical compositions) are joined into 3D covalent structures.

(26) Feng, P.; Bu, X.; Stucky, G. D. *Nature* **1997**, *388*, 735–741.
(27) Wu, T.; Wang, X.; Bu, X.; Zhao, X.; Wang, L.; Feng, P. *Angew. Chem., Int. Ed.* **2009**, *48*, 7204–7207.

2. Experimental Section

2.1. Materials and General Methods. All reagents and solvents employed in these synthetic studies were commercially available and used as supplied without further purification. Solid-state reflectance spectra were recorded on a Shimadzu UV-3101PC UV−vis−NIR scanning spectrophotometer by using $BaSO_4$ powder as 100% reflectance reference. Powder X-ray diffraction (PXRD) data were collected using a Bruker D8-Advance powder diffractometer operating at 40 kV, 40 mA with Cu Kα ($\lambda = 1.5406$ Å) radiation (2θ range, 2−40°; step, 0.03°; scan speed, 60 s/step). Semiquantitative elemental analyses of the compounds were performed with a Philips FEI XL30 scanning electron microscope (SEM) equipped with an energy-dispersive spectroscopy (EDS) detector.

2.2. Synthetic Studies. 2.2.1. Synthesis of the Mixture of OCF-5-CuGaSnSe-DPM and OCF-40-CuGaSnSe-PR. $SnCl_2$ (30.4 mg, 0.160 mmol), $Ga(NO_3)_3$ (255.2 mg, 0.997 mmol), Se (177.7 mg, 2.251 mmol), $Cu(NO_3)_2\cdot 3H_2O$ (31.9 mg, 0.132 mmol), and dipiperidinomethane (DPM; 2.061 g, 11.305 mmol) were mixed with H_2O (2.977 g, 165.39 mmol) in a 23-mL Teflon-lined stainless steel autoclave and stirred for 0.5 h. The vessel was then sealed and heated to 200 °C for 9 days. After cooling to room temperature, pale-yellow octahedral crystals and red block crystals were simultaneously observed in ~1:1 ratio, estimated using an optical microscope. The mixture was ultrasonically treated and washed with ethanol to remove some amorphous solid and then dried in air for other measurements. Crystals of OCF-40-CuGaSnSe-PR were in the form of rhombic dodecahedra (Figure 1).

2.2.2. Synthesis of OCF-40-ZnGaSnSe-PR. $SnCl_2$ (34.9 mg, 0.184 mmol), $Ga(NO_3)_3$ (252.7 mg, 0.988 mmol), Se (176.3 mg, 2.233 mmol), $Zn(NO_3)_2\cdot 6H_2O$ (76.9 mg, 0.259 mmol), and DPM (2.074 g, 11.376 mmol) were mixed with H_2O (2.481 g, 137.8 mmol) in a 23-mL Teflon-lined stainless steel autoclave and stirred for 2 h. The vessel was then sealed and heated to 200 °C for 10 days. After cooling to room temperature, only yellow block crystals were obtained in a yield of about 115.3 mg. Elemental analysis (%), calcd for $[(Zn_4Ga_{14}Sn_2Se_{35})\cdot 12(C_5NH_{12})]$: C, 13.66; H, 2.76; N, 3.19. Found: C, 13.61; H, 2.57; N, 3.15.

2.2.3. Method To Enhance the Yield and Purity of OCF-40-CuGaSnSe-PR and OCF-40-ZnGaSnSe-PR. *Method I* (increasing reaction time): $SnCl_2$ (32.0 mg, 0.169 mmol), $Ga(NO_3)_3$ (258.6 mg,

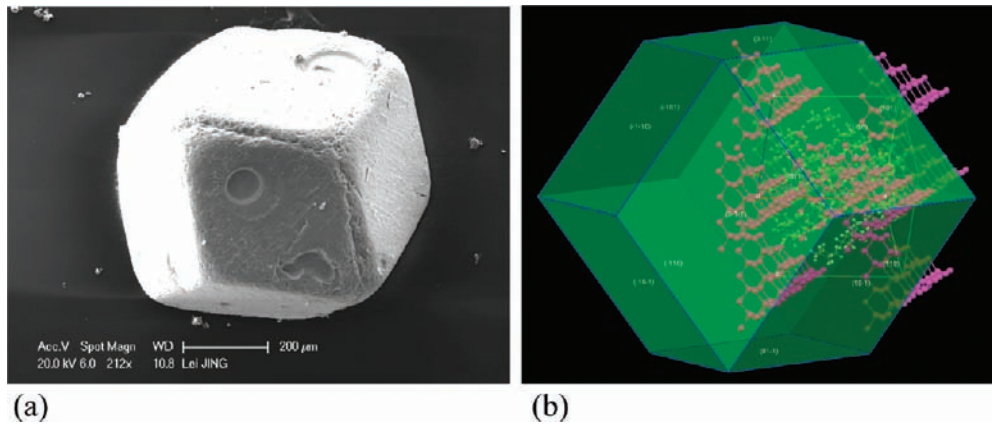

Figure 1. SEM pictures of OCF-40-CuGaSnSe-PR: (a) rhombic dodecahedron shape (in agreement with the predicated crystal morphology) and (b) from the internal crystal structure according to Bravais−Friedel−Donnay−Harker (BFDH) method.

1.011 mmol), Se (172.3 mg, 2.182 mmol), $Cu(NO_3)_2 \cdot 3H_2O$ (33.4 mg, 0.138 mmol), and DPM (2.051 g, 11.25 mmol) were mixed with H_2O (3.225 g, 179.16 mol) in a 23-mL Teflon-lined stainless steel autoclave and stirred for 1 h. The vessel was then sealed and heated to 200 °C for 15 days. After cooling to room temperature, only dark red block crystals were obtained in a yield of 221.2 mg. OCF-5-CuGaSnSe-DPM, which was observed with shorter reaction time, was completely converted into OCF-40-CuGaSnSe-PR. *Method II*: The synthesis procedure is similar to the one above, except that DPM was replaced with piperidine. Elemental analysis (%), calcd for $[(Cu_2Ga_{16}Sn_2Se_{35}) \cdot 12(C_5NH_{12})]$: C, 13.65; H, 2.76; N, 3.19. Found: C, 13.58; H, 2.52; N, 3.11. Unless noted, Method II was used for the preparation of OCF-40s in all different compositions.

The presence of multiple elements in OCF-5-CuGaSnSe-DPM and all variations of OCF-40s was confirmed by energy-dispersive X-ray (EDAX) spectroscopy performed on a SEM (see Supporting Information, Figure S1). The molar ratio of Cu:Ga:Sn in OCF-40-CuGaSnSe-PR determined by atomic absorption spectroscopy analysis is 1:8.263:1.124, and the molar ratio of Zn:Ga:Sn in OCF-40-ZnGaSnSe-PR is 1:3.593:0.525, in good agreement with results from single-crystal structure refinement based on significantly different atomic scattering power between Ga and Sn.

2.2.4. Synthesis of OCF-5-ZnGaSnSe-2-MPR and OCF-40-ZnGaSnSe-2-MPR. The procedure is similar to that for OCF-40-ZnGaSnSe-PR, except that piperidine was replaced with 2-methylpiperidine (Table S1, Supporting Information). The resulting products contain a very small amount of OCF-5-ZnGaSnSe-2-MPR and a large amount of OCF-40-ZnGaSnSe-2-MPR.

2.2.5. Synthesis of OCF-5-ZnGaSnSe-3-MPR. The synthesis procedure is similar to that for OCF-40-ZnGaSnSe-PR, except that piperidine was replaced with 3-methylpiperidine. The resulting product is pure.

2.2.6. Synthesis of OCF-40-CuGaSnSe-4-MPR. The synthesis procedure is similar to that for OCF-40-CuGaSnSe-PR, except that piperidine was replaced with 4-methylpiperidine.

2.2.7. Synthesis of OCF-40-ZnGaSnSe-4-MPR. The synthesis procedure is similar to that for OCF-40-ZnGaSnSe-PR, except that piperidine was replaced with 4-methylpiperidine.

2.2.8. Synthesis of OCF-40-MnGaSnSe-PR. The synthesis procedure is similar to that for OCF-40-CuGaSnSe-PR, except that $Cu(NO_3)_2 \cdot 3H_2O$ was replaced with $Mn(Ac)_2 \cdot 4H_2O$. A small amount of red crystals (OCF-40-MnGaSnSe-PR) was obtained.

2.2.9. Synthesis of OCF-40-CuGaSnS-PR. The synthesis procedure is similar to that for OCF-40-CuGaSnSe-PR, except that Se was replaced with S. A large amount of red crystals was obtained.

2.2.10. Synthesis of OCF-40-ZnGaSnS-PR. The synthesis procedure is similar to that for OCF-40-ZnGaSnSe-PR, except that Se was replaced with S. A large amount of pale-yellow crystals was obtained.

2.2.11. Synthesis of OCF-40-MnGaSnS-PR. The synthesis procedure is similar to that for OCF-40-MnGaSnSe-PR, except that Se was replaced with S. A small amount of red crystals (OCF-40-MnGaSnS-PR) and a large amount of yellowish, unidentified amorphous solids were obtained.

2.3. Single-Crystal X-ray Structure Determination. Crystallographic data of OCF-5-CuGaSnSe-DPM: tetragonal, $I4_1/acd$, $a = b = 23.9286(2)$ Å, $c = 42.0821(5)$ Å, $V = 24095.3(4)$Å^3, $Z = 8$, $2\theta_{max} = 48$ ($-27 \le h \le 27$, $-24 \le k \le 27$, $-48 \le l \le 48$), $T = 150$ K, 131 661 measured reflections, $R_1 = 0.0585$ for 4741 reflections ($I > 2\sigma(I)$), GOF = 1.060. Crystallographic data of OCF-5-ZnGaSnSe-2-MPR: tetragonal, $I4_1/acd$, $a = b = 24.1584(12)$ Å, $c = 41.931(4)$ Å, $V = 24472(3)$Å^3, $Z = 8$, $2\theta_{max} = 40$ ($-23 \le h \le 23$, $-23 \le k \le 23$, $-38 \le l \le 40$), $T = 150$ K, 46 728 measured reflections, $R_1 = 0.0484$ for 2855 reflections ($I > 2\sigma(I)$), GOF = 1.069. Crystallographic data of OCF-5-ZnGaSnSe-3-MPR: tetragonal, $I4_1/acd$, $a = b = 24.0693(3)$ Å, $c = 42.2601(10)$ Å, $V = 24482.6(7)$Å^3, $Z = 8$, $2\theta_{max} = 42$ ($-24 \le h \le 24$, $-24 \le k \le 24$, $-42 \le l \le 42$), $T = 150$ K, 52 078 measured reflections, $R_1 = 0.0684$ for 3287 reflections ($I > 2\sigma(I)$), GOF = 1.190. Crystallographic data of OCF-40-CuGaSnSe-PR: cubic, $I\bar{4}3m$, $a = b = c = 18.80190(10)$ Å, $V = 6646.69(6)$Å^3, $Z = 2$, $2\theta_{max} = 55$ ($-18 \le h \le 24$, $-24 \le k \le 24$, $-22 \le l \le 24$), $T = 150$ K, 26 479 measured reflections, $R_1 = 0.0328$ for 1151 reflections ($I > 2\sigma(I)$), GOF = 1.087. Crystallographic data of OCF-40-ZnGaSnSe-PR: cubic, $I\bar{4}3m$, $a = b = c = 18.89510(10)$ Å, $V = 6746.02(6)$Å^3, $Z = 2$, $2\theta_{max} = 60$ ($-17 \le h \le 25$, $-26 \le k \le 24$, $-26 \le l \le 26$), $T = 150$ K, 27 073 measured reflections, $R_1 = 0.0408$ for 1842 reflections ($I > 2\sigma(I)$), GOF = 1.115. Crystallographic data of OCF-40-MnGaSnSe-PR: cubic, $I\bar{4}3m$, $a = b = c = 18.8626(2)$ Å, $V = 18.8626(2)$Å^3, $Z = 2$, $2\theta_{max} = 50$ ($-22 \le h \le 10$, $-20 \le k \le 19$, $-12 \le l \le 21$), $T = 150$ K, 8954 measured reflections, $R_1 = 0.0417$ for 1119 reflections ($I > 2\sigma(I)$), GOF = 1.074. Crystallographic data of OCF-40-CuGaSnS-PR: cubic, $I\bar{4}3m$, $a = b = c = 18.4280(3)$ Å, $V = 6257.99(18)$Å^3, $Z = 2$, $2\theta_{max} = 50$ ($-10 \le h \le 21$, $-13 \le k \le 21$, $-17 \le l \le 19$), $T = 150$ K, 4820 measured reflections, $R_1 = 0.0538$ for 1025 reflections ($I > 2\sigma(I)$), GOF = 1.045. Crystallographic data of OCF-40-ZnGaSnS-PR: cubic, $I\bar{4}3m$, $a = b = c = 18.2580(15)$ Å, $V = 6086.4(9)$Å^3, $Z = 2$, $2\theta_{max} = 56$ ($-4 \le h \le 23$, $-1 \le k \le 24$, $-11 \le l \le 16$), $T = 150$ K, 4455 measured reflections, $R_1 = 0.0584$ for 1342 reflections ($I > 2\sigma(I)$), GOF = 1.061. Crystallographic data of OCF-40-MnGaSnS-PR: cubic, $I\bar{4}3m$, $a = b = c = 18.2580(15)$ Å, $V = 6086.4(9)$Å^3, $Z = 2$, $2\theta_{max} = 56$ ($-4 \le h \le 23$, $-1 \le k \le 24$, $-11 \le l \le 16$), $T = 150$ K, 6203 measured reflections, $R_1 = 0.0426$ for 786 reflections ($I > 2\sigma(I)$), GOF = 1.146.

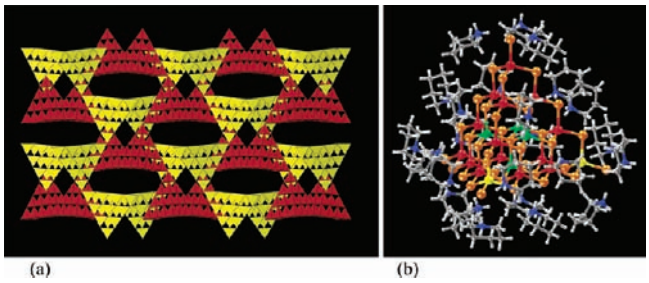

Figure 2. (a) Two-fold interpenetrated (red and yellow) 3D framework constructed by corner-sharing supertetrahedral T4 clusters in OCF-5-MGaSnSe (M = Cu, Zn). (b) Isolated supertetrahedral T4 cluster surrounded by 24 protonated piperidine molecules in OCF-40s (red, Ga; orange, Se/S; yellow, Sn; green, Zn or Mn or mixed Cu/Ga; blue, N; gray, C; white, H).

Single-crystal X-ray analysis was performed on a Bruker Smart APEX II CCD area diffractometer with nitrogen-flow temperature controller using graphite-monochromated Mo Kα radiation (λ = 0.71073 Å), operating in the ω and ϕ scan mode. The SADABS program was used for absorption correction. The structure was solved by direct methods, and the structure refinements were based on $|F^2|$. All atoms except those in disordered template molecules in OCF-5s were refined with anisotropic displacement parameters. The hydrogen atoms were generated geometrically. All crystallographic calculations were conducted with the SHELXTL software suites. CCDC reference numbers are 753143−753148, 765560, and 765561 for OCF-5-CuGaSnSe-DPM, OCF-5-ZnGaSnSe-2-MPR, OCF-5-ZnGaSnSe-3-MPR, OCF-40-CuGaSnSe, OCF-40-ZnGaSnSe-PR, OCF-40-MnGaSnSe-PR, OCF-40-CuGaSnS-PR, and OCF-40-ZnGaSnS-PR, respectively. These data can be obtained free of charge at www.ccdc.cam.ac.uk/conts/retrieving.html or from the Cambridge Crystallographic Data Centre, 12 Union Rd., Cambridge CB2 1EZ, UK; fax +44-1223/336-033; E-mail deposit@ccdc.cam.ac.uk. (CIF files are also available as Supporting Information.)

3. Results and Discussion

3.1. Transformation from 3D Covalent Framework to Discrete T4 Clusters. As shown in Table 1, isolated T4 clusters have been synthesized in a variety of compositions. It is, however, interesting to note that our original discovery of isolated T4 clusters in the Cu−Ga−Sn−Se system resulted from an unusual and unprecedented phenomenon in the metal chalcogenide chemistry: the hydrothermal transformation from the 3D covalent T4 framework into isolated 0D T4 clusters. Upon reacting $SnCl_2$, $Ga(NO_3)_3$, Se, $Cu(NO_3)_2 \cdot 3H_2O$, dipiperidinomethane (DPM), and deionized water under hydrothermal conditions (200 °C for 9 days), the pale-yellow octahedral crystals (OCF-5-CuGaSnSe-DPM comprising covalently linked T4 clusters) and dark red block crystals (OCF-40-CuGaSnSe-PR containing discrete T4 clusters, PR = piperidine) were obtained in ∼1:1 ratio. Longer reaction time led to OCF-40-CuGaSnSe-PR as the only product, suggesting the transformation from 3D covalent OCF-5-CuGaSnSe-DPM into molecular OCF-40-CuGaSnSe-PR. This is a totally unexpected observation, because the previous research has repeatedly shown that the polymeric framework, which OCF-5-CuGaSnSe-DPM has, is a far more favorable product under such synthesis conditions. The fact that such isolated T4 clusters can not only be synthesized, but at the cost of a well-known stable 3D OCF-5 framework, is truly extraordinary.

The mechanism for the above unusual transformation was revealed by single-crystal structure analysis, which shows completely disordered amine molecules in OCF-5-CuGaSnSe-DPM and highly ordered protonated piperidine ($[C_5H_{10}NH_2]^+$) in OCF-40-CuGaSnSe-PR. It is clear that the piperidinium cations came from the decomposition of DPM. With this knowledge, pure OCF-40-CuGaSnSe-PR can be synthesized directly by using piperidine as template with yield higher than that obtained by using DPM, as evidenced by PXRD (Figure S2, Supporting Information). Thus, one driving force for the transformation from 3D OCF-5-CuGaSnSe-DPM to molecular OCF-40-CuGaSnSe-PR is the gradual decomposition of DPM into piperidine, which causes the dissolution of covalent OCF-5 and subsequent reassembly into molecular OCF-40 (Figure S3, Supporting Information). The kinetics of the DPM decomposition and the associated 3D-to-0D conversion is dependent on the type of metal cations. For example, when replacing $Cu(NO_3)_2 \cdot 3H_2O$ with $Zn(NO_3)_2 \cdot 6H_2O$, the OCF-5 phase cannot be detected, and the pure OCF-40-ZnGaSnSe-PR is the only product, even when different reaction times are used. The subsequent synthesis of OCF-40s with other compositions is performed by using piperidine or substituted piperidine (Table 1).

3.2. Geometric and Charge-Density Matching between T4 Clusters and Organic Templates. OCF-5-CuGaSnSe-DPM and OCF-40-CuGaSnSe-PR comprise the same supertetrahedral T4 nanocluster $[Cu_2Ga_{16}Sn_2Se_{35}]$ with 18 bicoordinate Se^{2-} sites on six edges, 12 tricoordinate Se^{2-} ions on four faces, and one tetrahedral Se^{2-} at the core of the T4 supertetrahedron. The difference is that there are four monocoordinate terminal Se^{2-} ions at the four corners of the T4 supertetrahedron in OCF-40-CuGaSnSe-PR, whereas in OCF-5-CuGaSnSe-DPM, these corner Se sites are shared with other four adjacent clusters to form a 3-D extended open framework with two-fold interpenetrated diamond topology (Figure 2a), which was first found in the Cd−In−S system.[22]

The isolated clusters in OCF-40-CuGaSnSe-PR pack in a body-centered cubic (bcc) pattern with piperidinium cations occupying the intercluster space (Figure 3a; Figure S4, Supporting Information). Single-crystal structure refinement based

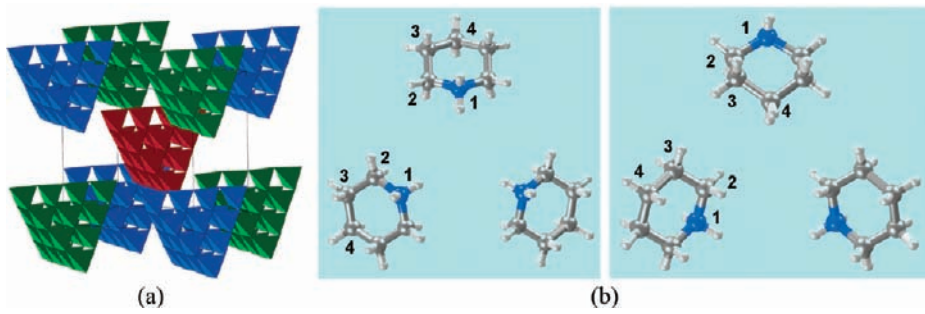

Figure 3. (a) Body-centered cubic packing pattern in one unit cell. (b) Spatial orientation of three adjacent piperidinium cations.

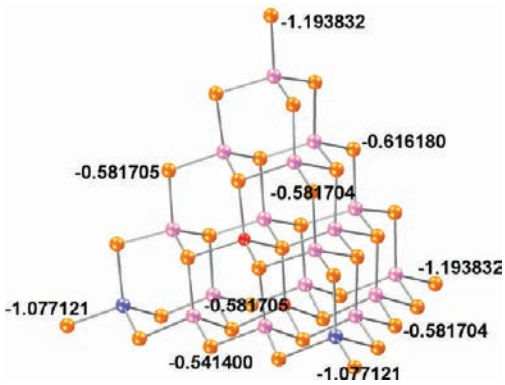

Figure 4. Mulliken charge distribution of Se^{2-} at the four corners and six edge-centers by RB3LYP/LANL2DZ theoretical calculation on OCF-40-CuGaSnSe-PR (pink, Ga; orange, Se; blue, Sn; red, Cu).

on the large difference in the scattering power between Sn^{4+} and Ga^{3+} shows that there are only two Sn^{4+} ions statistically distributed at two of four corner sites. To satisfy Pauling's electrostatic valence rule, the central tetrahedral Se^{2-} site is surrounded by two Cu^{+} ions and two Ga^{3+} ions to give a bond valence sum of 2+, consistent with the valence of Se^{2-}. OCF-40-ZnGaSnSe-PR is isostructural to OCF-40-CuGaSnSe, but the central Se^{2-} site is tetrahedrally coordinated to four zinc ions to satisfy Pauling's electrostatic valence rule. The Sn/Ga−Se bond distances at four corners in three selenide phases, OCF-40-MGaSnSe-PR (M = Mn, Cu, Zn), range from 2.4583 to 2.5146 Å, which lies between previously reported Sn−Se (2.490−2.521 Å)[9,27] and the Ga−Se bond lengths (2.379−2.418 Å).[28] Three sulfide phases, OCF-40-MGaSnS-PR (M = Cu, Zn, Mn), are isostructural to OCF-40-MGaSnSe-PR, but the shorter M−S bond lengths give rise to the smaller T4 cluster and smaller unit cells (Table 1).

While the single-crystal X-ray analysis of OCF-40-CuGaSnSe-PR produces only a statistically average structure with two Cu^{+} and two Sn^{4+} sites per cluster, the distribution of Cu^{+} and Sn^{4+} sites in each cluster is unlikely to be random from the chemical point of view. Ideally, two Cu^{+} sites bonded to the central Se^{2-} site should be located at positions closer to two corner Sn^{4+} sites so that the valence sum from cations to the anionic site is distributed as evenly as possible. The preliminary theoretical calculation on Mulliken charge distribution reveals the presence of more negative charge centers at the corners of the supertetrahedron and also at the center of each edge (Figure 4; Table S2, Supporting Information).

The fact that isolated T4 clusters can be obtained from the disintegration of covalently linked T4 clusters suggests the extraordinary stability of the isolated T4 clusters. Such a high stability comes from the perfect match between the piperidinium and the T4 clusters, in terms of charge density, geometry, and mutual interactions (electrostatic and hydrogen-bonding). In OCF-40-CuGaSnSe-PR, each Se^{2-} at the edge center of the supertetrahedron interacts with two piperidinium cations via a weak N−H···Se hydrogen bond, with the N···Se distance of 3.29 Å, and each corner Se^{2-} is bonded to three piperidiniums, with the N···Se distance of 3.11 Å (Figure 5), much smaller than the sum of Se and N van der Waals radii (3.41 Å). So each isolated T4 cluster is surrounded by a total of 24 piperidinium cations [4(3) + 6(2) = 24] (Figure 2b). Since each piperidinium has a Y-shaped connection to one corner Se^{2-} from one cluster and one central Se^{2-} on the edge center from another cluster, the negative charge (12−) per cluster exactly matches the positive charge (24+/2 = 12+) of piperidinium cations.

The above discussion about the perfect match between piperidinium cations and T4 clusters highlights the great significance of the choice of amines and of using charge-complementary metal cations ($M^{+}/M^{3+}/M^{4+}$ or $M^{2+}/M^{3+}/M^{4+}$) to tune the charge of the clusters. The incorporation of two Sn^{4+} ions into 2 of the 20 metal sites is critical for the crystallization of OCF-40 by reducing the charge of the T4 cluster from 14− in $[Cu_2Ga_{18}Se_{35}]^{14-}$ to 12− in $[Cu_2Ga_{16}Sn_2Se_{35}]^{12-}$. Indeed, in control experiments without any tin salt, OCF-40 could not be synthesized.

3.3. Solubility Behaviors and Stabilization of T4 Clusters with Surface Organic Cations. Because of their molecular nature, the solubility of OCF-40s is of particular interest. A large number of solvents have been examined in this work. It was found that OCF-40s have a rather peculiar solubility property. They are not soluble in many common aprotic polar or nonpolar organic solvents, such as chloroform, benzene, toluene, hexane, cyclohexane, petroleum ether, acetonitrile, and triethylamine. Neither are they soluble in common protic polar solvents, such as water, ethanol, methanol, and even aqueous CsCl (1 M) with high ionic strength. However, OCF-40s exhibit appreciable solubility in aprotic weak base solvents, such as DMF, DMSO, and piperidine. The resulting DMSO solutions were characterized by UV−vis adsorption spectroscopy (Figure 6), which shows that solutions of metal selenides exhibit broader adsorption bands than those of metal sulfides. One possible reason for the appreciable solubility in DMF and DMSO may be that they serve as hydrogen-bond acceptors for piperidinium to facilitate the dissolution of the solid samples, in addition to acting as good solvents for piperidine. Crystalline samples of OCF-40s are stable in air, and their solutions in DMF and DMSO are also stable when stored in capped vials. However, upon exposure to air for several days, an unidentified black powder is observed to precipitate from selenide solutions. OCF-

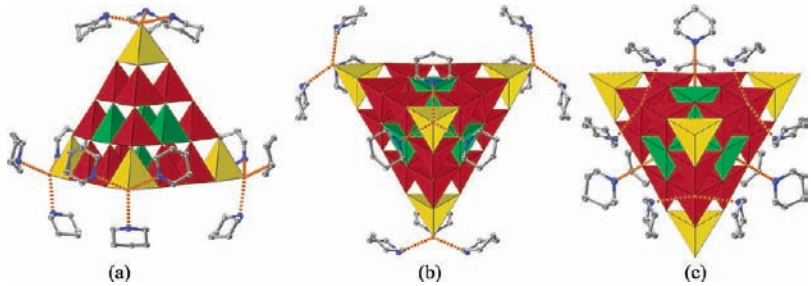

Figure 5. Strong N−H···Se hydrogen bond formed between corner Se^{2-} and protonated piperidine viewed along one side of the cluster (a) and down the C_3 axis (b), and edged Se^{2-} and protonated piperidine cations viewed down the C_3 axis (c).

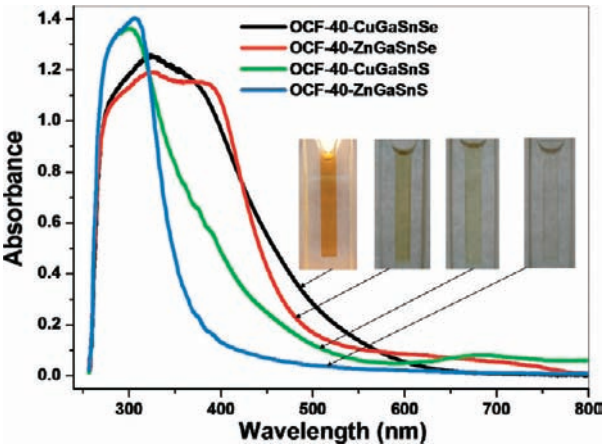

Figure 6. Effects of Cu^{+} vs Zn^{2+} and Se^{2-} vs S^{2-} on band structures in solution: UV−vis adsorption spectra of the filtrates of crystalline OCF-40s (15 mg) immersed and stirred in 5 mL of DMSO at room temperature.

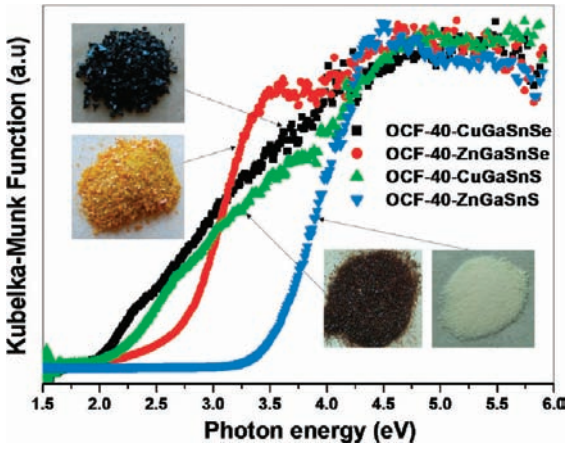

Figure 7. Effects of Cu^{+} vs Zn^{2+} and Se^{2-} vs S^{2-} on band structures in solid state: normalized solid-state UV−vis absorption spectra of OCF-40s. Insets are photos of the as-synthesized crystalline materials.

40s can be also digested in strong base solutions such as KOH (0.1 M), likely through the deprotonation of piperidinium cations.

Of particular interest is the apparent existence of a stable "ion pair" composed of one isolated T4 anion cluster and 12 piperidinium cations. OCF-40s have significant solubility in piperidine itself. However, the dissolution or dissociation behavior of OCF-40s in piperidine is different from that in DMSO. The dissolution of OCF-40-MGaSnSe-PR (M = Cu, Zn) in DMSO results in a significant increase in the electrical conductivity, whereas the dissolution of OCF-40-MGaSnSe-PR (M = Cu, Zn) in piperidine results in no change in the electrical conductivity. This suggests that, in DMSO, at least some of the dissolved species exist as negatively charged T4 clusters and positively charged piperidinium. On the other hand, in piperidine, the solid dissolves into neutral ion pairs, $[(T4)^{12-}\cdot 12(C_5H_{12}N)^{+}]$, which is unusual in metal chalcogenide chemistry. It reveals a new way to stabilize chalcogenide clusters, because in general chalcogenide clusters are stabilized by covalently attached organic ligands, not organic cations bonded to the cluster surface through electrostatic force, as reported here. It also further supports the strong interaction

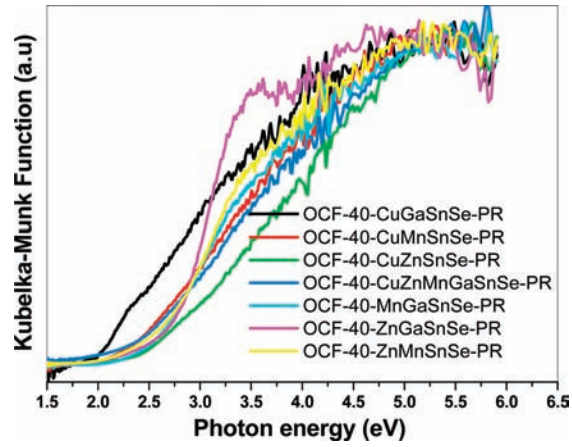

Figure 8. Effects of different metal ions (Mn^{2+}, Cu^{+}/Mn^{2+}, Zn^{2+}/Mn^{2+}, Cu^{+}/Zn^{2+}, and $Cu^{+}/Zn^{2+}/Mn^{2+}$) on band structures: normalized solid-state UV−vis absorption spectra of OCF-40-MnGaSnSe-PR, OCF-40-CuMnGaSnSe-PR, OCF-40-ZnMnGaSnSe-PR, OCF-CuZnGaSnSe-PR, and OCF-40-CuZnMnGaSnSe-PR.

between piperidinium and the T4 cluster. Such strong interaction greatly stabilizes the discrete T4 cluster and creates a thermodynamic driving force for the extraordinary transformation from 3D OCF-5-CuGaSnSe-DPM to molecular OCF-40-CuGaSnSe-PR.

3.4. Tunable Optical Properties in Solution and Solid State. These isostructural OCF-40s show a remarkable effect of different d^{10} metal ions (Cu^{+} and Zn^{2+}) and chalcogen anions (Se^{2-} and S^{2-}) on the sample colors and band gap of semiconductor materials. The dark red selenide sample of OCF-40-CuGaSnSe-PR has a wider UV−vis adsorption peak than the yellow sample of OCF-40-ZnGaSnSe-PR (Figure 7). A similar difference is also found in sulfides between OCF-40-CuGaSnS-PR and OCF-40-ZnGaSnS-PR. The solid-state diffuse reflectance spectra obtained on a Shimadzu UV-3101PC double-beam, double-monochromator spectrophotometer using $BaSO_4$ powder as 100% reflectance reference reveal that OCF-40s are semiconductors with a range of band gaps: OCF-40-CuGaSnSe-PR, 1.91 eV; OCF-40-ZnGaSnSe-PR, 2.71 eV; OCF-40-CuGaSnS-PR, 2.11 eV; and OCF-40-ZnGaSnS-PR, 3.59 eV (as calculated from reflectance data by using the Kubelka−Munk function).[29] It is clear that, with other factors being equal, Cu^{+} and Se^{2-} give materials with much lower band gaps.

In the field of chalcogenide cluster chemistry, there are a rather limited number of examples in which clusters exist in both discrete and covalently linked forms.[30] Thus, OCF-5s and OCF-40s reported here present a unique opportunity to examine the effect of structures (0D vs 3D) on the optical properties. The significant difference in band gap between molecular OCF-40-CuGaSnSe-PR (1.91 eV) and 3D covalent OCF-5-CuGaSnSe-DPM (1.50 eV) is likely caused by a quantum confinement effect. The zero-dimensional nanoscale cluster is expected to exhibit a blue-shift in adsorption compared with covalent frameworks or condensed phases with comparable compositions.

In addition to offering tunability in the charge of the cluster, which is essential for successful crystallization, the quaternary

(28) Bu, X.; Zheng, N.; Wang, X.; Wang, B.; Feng, P. *Angew. Chem., Int. Ed.* **2004**, *43*, 1502–1505.

(29) Wendlandt, W. W.; Hecht, H. G. *Reflectance Spectroscopy*; Interscience: New York, 1966.

(30) (a) Melullis, M.; Clérac, R.; Dehnen, S. *Chem. Commun.* **2005**, 6008–6010. (b) Manos, M. J.; Iyer, R. G.; Quarez, E.; Liao, J. H.; Kanatzidis, M. G. *Angew. Chem., Int. Ed.* **2005**, *44*, 3552–3555.

Scheme 1. Molecular Structures and Names of Eight Similar Amine Templates, Including Their Abbreviations

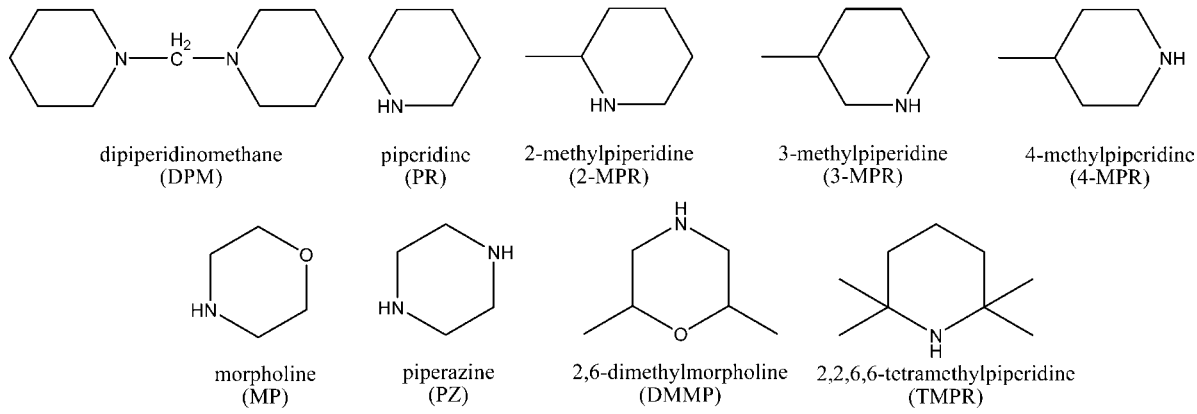

Table 2. Effects of Different Amine Templates on the Competing Crystallization of OCF-5s and OCF-40s

	PR	2-MPR	3-MPR	4-MPR	MP	PZ	DMMP	TMPR
$Zn(NO_3)_2$	OCF-40	OCF-5 (minor), OCF-40 (major)	OCF-5	OCF-40	OCF-5	OCF-5	OCF-5	OCF-5
$Cu(NO_3)_2$	OCF-40			OCF-40				OCF-5

cluster composition provides a convenient way to tune electronic properties of discrete T4 clusters by allowing the variation of the cluster compositions on the basis of types of metal ions and chalcogenide anions (S^{2-} or Se^{2-}). In the above, we have already shown that the use of Cu^{+}, Zn^{2+}, S^{2-}, and Se^{2-} makes it possible to tune the electronic band gaps over a wide range. As shown in Table 1, other metal ions such as Mn^{2+} can also be employed to further tune the semiconducting properties of the T4 cluster compound, as evidenced by the syntheses of OCF-40-MnGaSnSe-PR and OCF-40-MnGaSnS-PR. In addition, it is possible to develop even more complex cluster compositions by combining two or more low-valent metal ions (Cu^{+}, Zn^{2+}, Mn^{2+}) in the reaction system. Various permutations of these metal ions have allowed the synthesis of OCF-40-CuZnGaSnSe-PR, OCF-40-ZnMnGaSnSe-PR, OCF-40-CuMnGaSnSe-PR, and OCF-40-CuZnMnGaSnSe. All of these compositions have been verified by qualitative elemental analysis using EDAX (Figure S1). Solid-state UV−vis adsorption measurement also shows the tunable band gap (Figure 8).

3.5. Effects of Organic Templates on the Competing Crystallization of OCF-5 vs OCF-40 and on Properties of OCF-40. While much of this work centers on controlling semiconducting properties by varying the composition of T4 clusters, we are also interested in the role of the organic component in structural control and in modifying the properties (e.g., solubility and stability) of the solids. To this end, we have further investigated the effect of various piperidine-like molecules on the final structures. Seven amines (Scheme 1) were chosen to replace piperidine in the hydrothermal synthesis. These amines possess different basicity and steric hindrance. It is observed that similar reaction processes, but with different amines, lead to two types of frameworks, OCF-5s and OCF-40s (Table 2). Their phase purity and structure are verified by PXRD (Figure S5) and single-crystal XRD.

As described above, the formation of discrete T4 clusters (OCF-40) faces inherent competition for the crystallization of covalently linked T4 clusters (OCF-5). We have already shown that the reaction time and the type of metal ions have an effect on whether OCF-5 or OCF-40 (or both) will be formed. Here, we have also found that the type of organic templates can dictate whether OCF-5 or OCF-40 will be formed. Before discussing the individual roles of organic amines, it is useful to give an overview of how amines behave in chalcogenides of various dimensionality. In 3-D chalcogenide frameworks, extra-framework protonated amines are almost always disordered to the extent that it is impossible to locate them in the crystallographic analysis. This suggests that the role of amines is mainly for charge-balancing and pore-filling and that the formation of 3-D frameworks is more tolerant of small variations in the size and shape of amines. In comparison, amines in low-dimensional chalcogenide structures are generally ordered, and there is a better match between structural features of amines and the chalcogenide units. Being zero-dimensional, OCF-40 represents an extreme case. In general, the formation of low-dimensional chalcogenide units, 0-D in particular, has a more stringent requirement for the organic amines, which explains why OCF-5 tends to occur more often than OCF-40 in this work.

The template amines with high steric hindrance and strong protonation ability easily give OCF-5 with the 3D covalent framework, while 2-methylpiperidne and 4-methylpiperidine induce the formation of OCF-40 with discrete clusters. This is

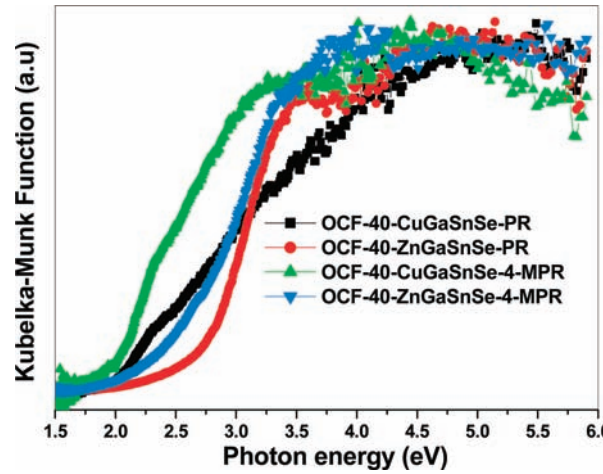

Figure 9. Effects of surface organic templates on band structures: normalized solid-state UV−vis absorption spectra of OCF-40-CuGaSnSe-4-MPR (band gap 1.80 eV) and OCF-40-ZnGaSnSe-4-MPR (band gap 2.60 eV), compared to OCF-40-CuGaSnSe-PR and OCF-40-ZnGaSnSe-PR.

because it is easier to fit bulky amines within the cavities of 3D OCF-5 than to fit them in an orderly manner on the surface of OCF-40. This point is further highlighted by comparing 3-methylpiperidine with 2- or 4-methylpiperidine.

A detailed analysis of the tripiperidinium aggregates near the corner of T4 cluster indicates that the 3-position in piperidine exhibits a much higher steric hindrance than the 2- or 4-position. (Figure 3b), making it difficult to arrange multiple 3-methylpiperidiniums around the cluster surface. It is worth noting that the 4-position methyl group gives a significantly larger unit cell, which is likely related to the two distinct orientations of methyl groups in the chair configuration. Such orientational disorder of 4-methylpiperidine leads to a lower crystal quality, and yet the weakening in the packing force contributes to the faster dissolution rate and increased solubility of 4-methylpiperidine-templated OCF-40 in piperidine, as compared to piperidine-templated OCF-40. Also worth noting is that the substitution of piperidinium by 4-methylpiperidinium in OCF-40s leads to a significant change in electronic properties (Figure 9).

4. Conclusions

In conclusion, we have synthesized and characterized a family of discrete chalcogenide supertetrahedral T4 clusters ($M_xGa_{18-x}Sn_2Q_{35}^{12-}$, $x = 2$ or 4; M = Mn, Cu, Zn; Q = S, Se) with tunable electronic and optical properties. By doubling the size of the previously known T3 cluster (in terms of the number of metal sites), these molecular T4 clusters are currently the largest exact fragment of the cubic ZnS-type lattice. The synthetic success demonstrates the great potential of our synthetic strategy based on charge-density tuning (by using multiple charge-complementary metal cations) in the generation of large chalcogenide clusters and their subsequent crystallization. Specifically, the introduction of tetravalent metal ion Sn^{4+} into the corners of M−Ga−Q (M = Cu, Zn, Mn; Q = Se, S)-based T4 chalcogenide clusters allows the lowering of charge density of the cluster to an optimum value that matches perfectly with the templating organic cations. Resulting soluble molecular clusters exhibit a wide range of electronic band properties. The synthesis of such clusters demonstrates the feasibility of continued success in the quest for even larger tetrahedral chalcogenide clusters that will eventually seamlessly blend the size gap between chalcogenide clusters and colloidal semiconductor nanoparticles.

Acknowledgment. We thank the NSF (P.F., CHEM-0809335; X.B., DMR-0846958) and Research Corporation (X.B., CC6593) for support of this work. P.Y. is a Camille Dreyfus Teacher Scholar, and X.B. is a Henry Dreyfus Teacher Scholar.

Supporting Information Available: Additional figures, crystallographic data including positional parameters, thermal parameters, and bond distances and angles (PDF, CIF). This material is available free of charge via the Internet at http://pubs.acs.org.

JA102688P